

Second sound in bursting freely suspended smectic-A films

Frank Müller, Christian Bohley, and Ralf Stannarius

Institute of Experimental Physics, Otto-von-Guericke University, 39016 Magdeburg, Germany

(Received 9 October 2008; published 15 April 2009)

We describe the bursting of macroscopic spherical bubbles formed by smectic liquid crystals. During rupture, strong light scattering is observed. It is suggested here that peristaltic undulations of the films are responsible for this scattering. This phenomenon distinguishes bursting smectic films from bursting soap films. The dynamics of these mechanical waves are strongly influenced by the internal layered structure of the smectic films, viz. by the elasticity of the molecular layers, expressed by the smectic layer compression modulus B . We study experimentally the optical properties of bursting smectic films by means of optical transmission measurements and laser scattering. The typical wavelength range of the propagating peristaltic waves is in the micrometer range. The wavelength spectrum rather is independent of the initial film thickness δ , but the scattering intensity strongly depends on δ .

DOI: [10.1103/PhysRevE.79.046315](https://doi.org/10.1103/PhysRevE.79.046315)

PACS number(s): 47.20.Dr, 42.25.Fx, 68.60.Bs

I. INTRODUCTION

A. Rupture of liquid films

Thin liquid films represent an interesting class of structures in soft-matter physics with unique features, owing to the existence of two adjacent liquid-air interfaces, the extremely large surface to volume ratio and their quasi-two-dimensional geometry. Static properties of such films are quite well understood. Dynamical processes, on the other hand, reveal several interesting unexplained phenomena. Examples from everyday life are the rupture of soap bubbles and aging of foams, and in biological systems the fusion of cells or the motion of liposomes in flow fields. Despite of experimental and theoretical works [1–11], many fundamental questions concerning the rupture of such films are still open.

Here, we describe the rupture of bubbles formed by smectic-A mesogenic material. Thin freely suspended films of thermotropic smectics are geometrically very similar to soap films. Their internal composition is different; a regular molecular layer structure exists in contrast to common soap films. This internal layer structure has at least two consequences for the behavior of smectic films that distinguish them from soap films. First, smectic films in equilibrium have a uniform film thickness, given by an integer number of discrete layers, and second, elastic forces related to the deformation of these layers enter the dynamic equations. One of these consequences, the propagation of certain types of mechanical waves during rupture, is analyzed in this study.

The commonly accepted model describing the rupture of planar soap films (e.g., [1–5]) is as follows:

- (i) a small hole in the film is formed spontaneously or after initiation,
- (ii) this hole in the film grows, whereby its edge moves with constant velocity in an inviscid material,
- (iii) a rim, separating the hole from the film, collects the film material during rupture, and
- (iv) film elements far from the rim stay at rest and remain undisturbed until they are absorbed by the proceeding rim.

Actually the bursting of soap films is more complicated; for example, McEntee and Mysels [7] and Frankel and Mysels [8] reported on disturbances in front of the moving rim (the so-called aureoles).

Starting from a momentum balance, the force at the film edge arising from the reduction in surface energy is related to the change in linear momentum of the rim material. The velocity of the rim in a smectic film of uniform thickness δ , surface tension γ , and density ρ is calculated to be [4]

$$v_c = \sqrt{\frac{2\gamma}{\rho\delta}}. \quad (1)$$

We will refer to this relation as Culick's equation in the following text. The factor of 2 reflects the existence of two surfaces (upper and lower) of the film. Strictly, in smectic films one has to use the film tension τ [12] that replaces 2γ in the numerator. It is related to the surface tension γ of the smectic material by $\tau = 2\gamma + \Delta p\delta$, where $\Delta p = \gamma/R_m$ is the pressure difference between the interior of the film and ambient pressure due to the curvature of the meniscus [13–17] and R_m is the radius of curvature of the meniscus (see, e.g., [18]).

From a dynamic point of view, there are no qualitative differences between the rupture of spherical and planar films. Culick's relation for the rim velocity still holds for spherical bubbles, at least when the film thickness is uniform everywhere. The rim is forced to follow essentially the bent shape of the bubble because of the resistance of the surrounding air to a lateral displacement of the film, normal to its plane. Investigations of the rupture of spherical soap films have been performed by Pandit and Davidson [11]. In bursting thermotropic smectic-A films, many similarities to soap films are found. In particular, the validity of Culick's velocity has been tested in experiments with smectic bubbles [19,20]. However, there are also striking differences to soap film rupture. In these experiments [19], we have found a darkening of smectic-A bubbles of micrometer film thickness during rupture when observed in transmission. Similarly, the bursting bubbles become much brighter under indirect illumination. This phenomenon has not been observed in comparable experiments with soap bubbles [20], and it has not been described in literature on soap films either. Thus, we hypothesize that the scattering is owed to the inherent layer structure of smectic-A free standing films.

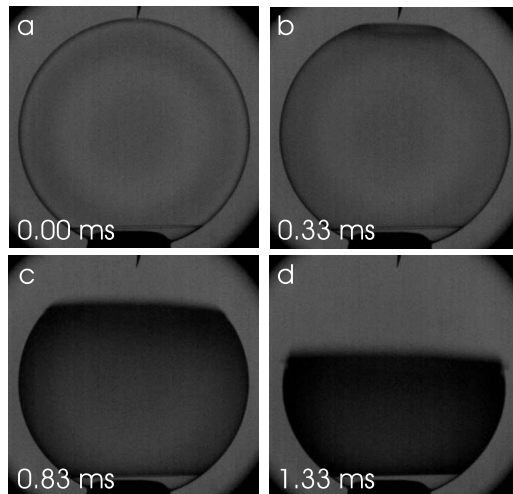


FIG. 1. Rupture of a smectic bubble with a film thickness δ of 1840 nm. The initial bubble radius was 5.4 mm. After puncture (at the top), one observes the opening of a hole and the motion of the edge downward. Furthermore, the images show a gradual darkening of the remaining part of the bubble in transmitted light due to scattering. The whole process takes place in less than 2 ms. The images are background corrected and contrast has been enhanced.

B. Mechanical waves in thin liquid films

Figure 1 shows a typical burst of a smectic bubble, initiated by a needle that is punctured through the top of the bubble. The rupture was observed with a fast camera at 15 000 frames per second (fps) in transmission. The bubble was illuminated with parallel monochromatic green light of wavelength $\lambda=535$ nm.

We propose that the scattering that leads to the darkening of transmission images of bursting smectic films is caused by undulations of the film-air interfaces. The undulations of both film surfaces are elastically coupled to each other and to the internal layer structure by the smectic layer compression elasticity. This is in contrast to the established soap film model, which predicts that film elements far from the rim remain undisturbed and at rest. Arguments that support our hypothesis will be provided in this work. In general, there are different types of undulation modes that can travel along a thin liquid film. They are distinguished by the symmetries of the undulations of upper and lower film surfaces and by the modulations of a potential inner layer structure of the film. Two modes of traveling waves on thin soap films have been described already by Taylor [5]. In the first type, the two film surfaces fluctuate in phase (similar to the bending or undulation mode shown in Fig. 2 for the smectic films). A dispersion-free velocity

$$v_u = \sqrt{\frac{2\gamma}{\rho\delta}} \quad (2)$$

has been derived for these so-called antisymmetric undulations. In smectic films, one expects the same type of antisymmetric waves to occur. Since undulations of this type leave the film thickness practically unchanged, they are not affected by the compression elasticity of the smectic layers.

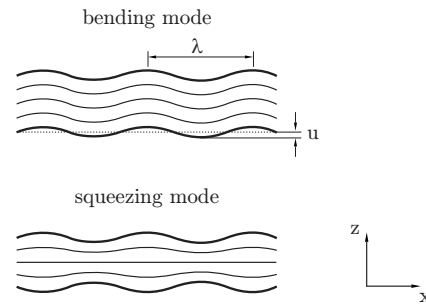


FIG. 2. Schematic sketch of two types of undulations of the surfaces in smectic films.

A comparison with Eq. (1) shows that such waves travel practically with the same speed as the progressing edge of the hole during film rupture. They are thus too slow to affect the bursting film. In smectic A, an additional term related to elastic distortions of the director, on the order of $K_{11}q^2\delta$, adds to the surface tension term 2γ in the numerator. K_{11} is the splay elastic constant of the material and $q=2\pi/\lambda$ is the in-plane component of the wave vector of undulations with wavelength λ . For wavelengths in the micrometer range which cause the scattering of bursting smectic films (cf. Sec. III B), the elastic energy term related to splay distortions of the director is about 2 orders of magnitude lower than the surface-tension contribution. It may therefore be neglected here.

The second type of waves in liquid films described by Taylor is symmetric surface undulations [the so-called peristaltic waves (cf. Fig. 2)]. The velocity assigned to this type of waves is

$$v_p = \sqrt{\frac{\gamma\delta}{2\rho}}$$

when a pure water film is considered and the elasticity of the surfactant layers is not taken into account. Their propagation velocity depends on the in-plane wave-vector component q . Experiments by Lucassen *et al.* [21] showed that such waves do not play a role in soap films when one allows for the elastic contributions of the surface layers. When the elasticity of the surfactant films is taken into account, a velocity

$$v_{sf} = \sqrt{\frac{2E_{sf}}{\rho\delta}} \quad (3)$$

is obtained [21,22]. The elasticity of the surface films E_{sf} replaces the surface tension γ in the equation for antisymmetric undulations. Both quantities are on comparable order of magnitude; consequently, these waves will not be much faster than the rim either.

In smectic-A films, such contributions of surface elasticity are absent. However, the peristaltic waves with symmetric surface fluctuations modify the local film thickness (Fig. 2). These waves couple to the internal layer structure of smectic films, and they lead to thickness distortions of the smectic layers.

All these types of undulations are relevant, for example, for light scattering experiments [23] or x-ray scattering of smectic free standing films (see, e.g., the review by de Jeu

[24] and references therein). Starting from the hydrodynamic theory of smectic phases [25], models have been developed that describe the fluctuations of thin smectic films by combining the bulk elastic contributions (layer compression modulus B and orientational elastic constant K) with contributions from the surface tension. The layer and surface fluctuations have been analyzed theoretically in several studies (e.g., [26–33]) and experimentally by x-ray diffuse scattering and specular reflectivity [34–36].

The two basic modes of bending and squeezing can be constructed for smectic films in analogy to soap films, as sketched in Fig. 2, and of course linear superpositions of these modes occur. Owing to the internal structure of the films, the surface fluctuations alone are not sufficient to describe the dynamic properties of mechanical waves on the film. One has to consider in general a superposition of modes with different normal components of the wave vector [31]. In smectic films, the velocity of squeezing (peristaltic) modes is strongly influenced by the layer elasticity. These layer undulations are related to the phenomenon of second sound [18,37], which is a peculiarity of smectic phases. First sound, i.e., ordinary longitudinal acoustic waves that are related to a compressibility of the liquid and to a change in its density, travels at velocities on the order of km/s [25,38]. Such sound waves, if generated during the impact of the moving rim onto the resting film material, lead only to very small density variations in the film and they are not observed optically in our experiments. Second sound, on the other hand, is found in liquids with layered structure [37] when the propagation direction of the wave is neither parallel nor perpendicular to the smectic layer but at an oblique angle to the layers. It has a characteristic propagation velocity on the order of $v_{ss} = \sqrt{B/\rho}$. With $B \approx 10^7$ Pa and $\rho \approx 10^3$ kg/m³, this velocity can be roughly 1 order of magnitude faster than the velocity of the rim of a bursting film. We will focus on this type of waves in the interpretation of the scattering experiments.

II. EXPERIMENTAL SETUP

The commercial liquid crystal 8CB (4'-*n* octyl-biphenyl-4-carbonitrile) with the phase sequence crystalline 21.5 °C smectic-A 33.5 °C nematic 41.5 °C isotropic was used in the experiments. It has been obtained from SYNTHON Chemicals and used without further purification. The experiments were performed at 26 °C, where 8CB is in the smectic-A phase. The preparation of the bubbles has been described earlier [19,20]: a thin smectic free standing film is spread over the open end of a cylindrical capillary. The bottom part of the capillary is connected to a syringe, which is used to press air into the capillary and thus to inflate a smectic bubble. At sufficiently low inflation speeds (total inflation time is approximately 1 min for a bubble of 10 mm diameter), the smectic film thickness is constant or contains only few discrete layer steps. After inflation, inhomogeneous bubbles are left to equilibrate for about 0.5 h then the film thickness is optically uniform. For 8CB it is typical that in films of inhomogeneous thickness, the thinnest film region grows and finally covers the whole film. Even though we cannot determine the film thickness with a resolution of

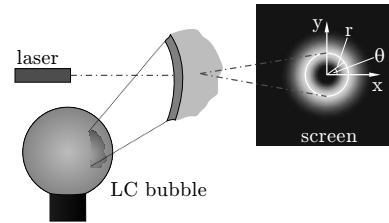


FIG. 3. Schematic sketch of the scattering experiment. Actually, the laser penetrates the bubble twice at opposite sides. The wavelength of the laser was 670 nm. The right-hand side shows a sketch of the scattering profile on a screen placed behind the bubble.

single-layer steps (the accuracy of thickness measurements in the bubbles is approximately three layers), we can assume that the final film thickness is uniform on a molecular scale.

Parallel monochromatic light is used for illumination of the bubbles. The initial film is photographed with a Nikon Coolpix 995 digital camera. The transmission profile of a bubble is influenced by the interference of light passing the smectic film directly and light that is reflected twice at the front and rear film surfaces. A quantitative comparison to calculated transmission profiles yields the initial film thickness as the only fit parameter. This method has been developed and described earlier [39].

The rupture is initiated with a needle pierced into the top of the bubble. After puncture, the light scattering of smectic-A films is observed with the setup sketched in Fig. 3. A 670-nm-wavelength laser beam is pointed through the center of the bubbles onto a semitransparent screen placed on the opposite side, in a distance $D=5.6$ cm from the bubble center. The scattering profiles on this screen were recorded with a fast camera (PHOTRON Ultima APX). Typically, the complete rupture takes less than 3 ms; thus, frame rates of 15 000 fps are necessary for sufficient temporal resolution of the scattering process. Alternatively, we have recorded transmission images of the bubbles by means of the same fast camera mounted on a K2 (INFINITY) long-range microscope (see, e.g., Figs. 1 and 4).

III. RESULTS

A. Transmission images of bursting smectic bubbles

Thick smectic films become opaque in transmission during rupture [19]; a typical example can be seen in Fig. 1. The opacity depends strongly on the initial film thickness δ . For $\delta < 400$ nm, no darkening can be detected. If the initial film thickness is greater than ≈ 700 nm, the darkening appears instantaneously and homogeneously over the entire film.

Figure 4 shows the rupture of a smectic bubble with two regions of different film thicknesses, separated by a thickness step that contains dislocations. At the moment of puncture, this horizontal border [black line in Fig. 4(a)] was slightly above the equator of the bubble. The film thickness in the top part ($\delta=1.49$ μm) is lower than in the bottom region ($\delta=5.63$ μm). Before the edge of the hole hits the dislocation at the film thickness step, light scattering occurs only in the top region of the film. Obviously, the peristaltic waves are reflected or absorbed at the film thickness step. The bottom

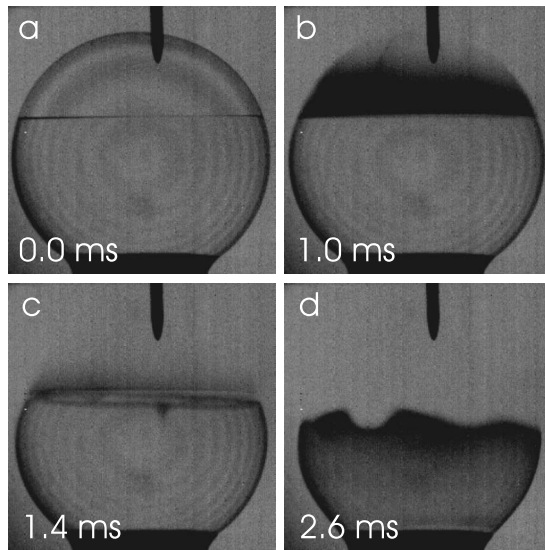


FIG. 4. (a)–(d) Rupture process of a bubble with significantly different film thicknesses δ in two regions, separated by a dislocation step. During rupture, the border between the two areas of uniform film thicknesses is displaced only slightly, unless it is reached by the rim. The film undulations are reflected or absorbed at the step. Darkening of the bottom part takes place only after the rim enters the uniform bottom film region. The blurred upper edge in the thin film regions (b) and (c) is an artifact, a slight afterimage of the camera. It does not occur in the bottom region where the rim moves slower. The undulation of the edge in (d) is a characteristic phenomenon observed when the rim passes a large film thickness step.

part becomes opaque as soon as the rim has passed the dislocation line separating the two regions. There is no qualitative difference in the scattering of both areas.

B. Laser scattering experiments

In order to understand the scattering of light by the bursting film, the transmission of a laser beam during the rupture

process has been recorded. The scattered laser beam profiles are shown in Fig. 5 for three bubbles with initial film thicknesses δ of 770 nm, 1.805 μm , and 4.66 μm , respectively. The time axis runs from left to right. In the first set of images taken immediately after puncture [(a), (e), and (i)], the primary laser beam is seen in the center. In the thin film, the scattering intensity is comparably low, and the primary beam remains visible during the burst. The scattering increases with increasing initial film thickness δ . In the case of the thick film ($\delta=4.66 \mu\text{m}$), the primary beam vanishes completely until the rim of the bursting film has passed the beam.

The scattering profile is on average axially symmetric around the primary beam. For a quantitative analysis, the scattering intensity belonging to the equal scattering angles $\phi=\arctan r/D\approx r/D$ is integrated. Here, D is the distance from the center of the bubble to the screen and r is the distance to the primary beam position on the screen (cf. the definition of geometrical parameters in Fig. 3). Actually, the laser beam passes the spherical film twice; the distance from the screen to the scattering film is somewhat larger than D (approximately by the bubble radius $R_{\text{bubble}}\approx 4 \text{ mm}$) for the first passage and somewhat smaller than D (by R_{bubble}) for the second passage. The resulting deviations on the order of 10% are not relevant for the qualitative and semiquantitative analyses of the scattering profiles. The integral intensity

$$I(r,t) = \int rI(\theta,r,t)d\theta \quad (4)$$

is calculated for every image in the series. This yields the dependence of scattered light intensity on time and scattering angle. In images 5, 6, and 7, the inner zone corresponding to the primary beam diameter has been clipped. In the remaining part, a background correction has been performed: the intensity $I_0(r,0)$, obtained before puncture, has been subtracted from all intensity profiles $I(r,t)$, in order to extract the contributions of the light scattered by the bursting film only. The time-dependent scattering profiles contain informa-

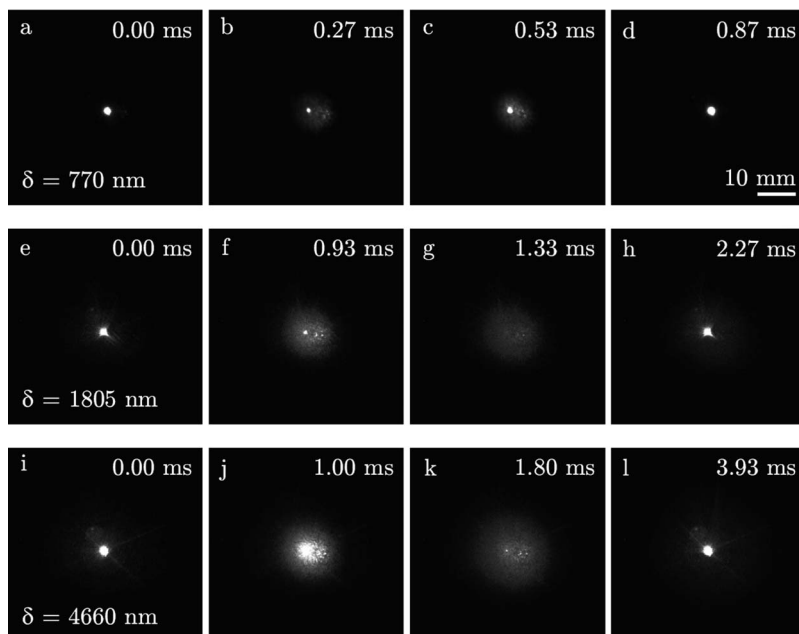


FIG. 5. Laser beam profile on a screen during the rupture of three films with different film thicknesses. The laser wavelength was 670 nm. The screen was placed 56 mm from the bubble center, opposite to the laser.

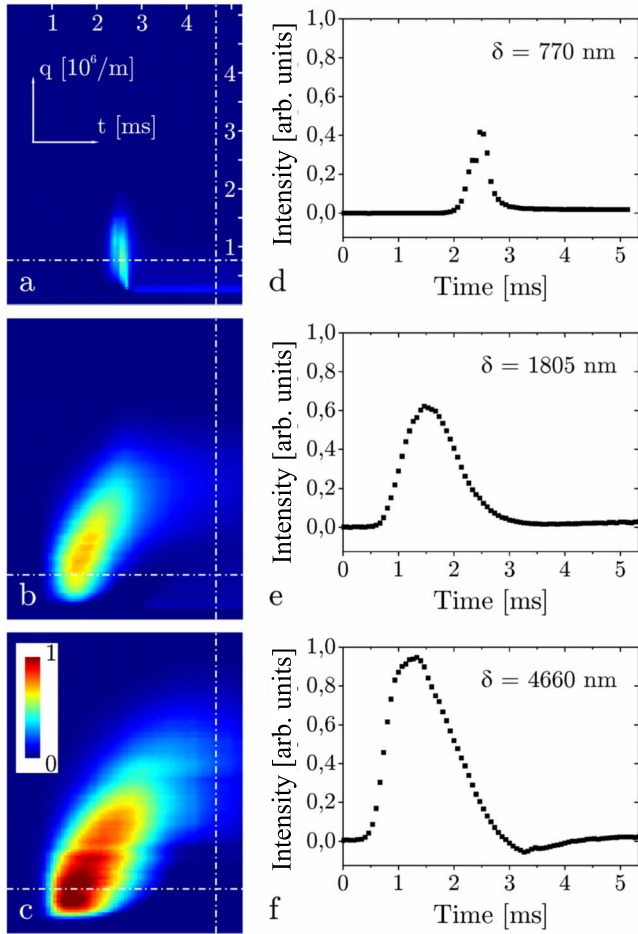


FIG. 6. (Color online) Dependence of the scattering intensity on the wave vector q and time for three different film thicknesses. The diagram refers to the cross section along the horizontal dashed-dotted line in the intensity plot to the left. The intensity of the scattered light depends strongly on the initial film thickness. Intensities belonging to equal wave numbers have been integrated using Eq. (4).

tion about the wavelengths of the film thickness modulations in the film. Of course, the relation between scattering profile and wavelengths of the undulations can be made only in crude approximation. The scattering intensity is high and the primary beam practically vanishes in thick films. We deal with multiple scattering, so that the intensity profile gives only some order of magnitude of the wavelengths of the film undulations.

Results are presented in Fig. 6. The figure shows the scattering of the same bubbles as in Fig. 5 (film thicknesses of 770 nm, 1.805 μm , and 4.66 μm). The pseudocolor surface plots visualize the temporal evolution of the radial scattering intensity. The time axis runs from left to right. Under the simplifying assumption that the scattering is due to periodic undulations of the film with wave number q , we express the radius r in the abscissa by

$$q = \frac{2\pi}{\lambda} = \frac{2\pi r}{\lambda_1 D}. \quad (5)$$

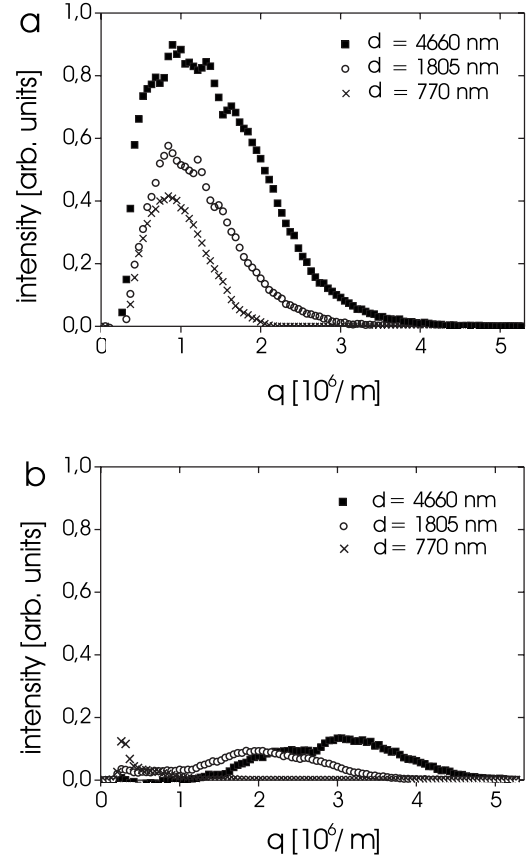


FIG. 7. Intensity profiles of the scattered laser light. (a) shows the cross section at the moment of maximum scattering intensity and (b) corresponds to the vertical dashed-dotted lines in Fig. 6, at a time when the rim has already passed the laser beam.

Here, λ_1 is the wavelength of the laser light and λ represents the wavelength of the film undulations. The first part of this equation defines q and the second part reflects the relation between q and the scattering angle ϕ .

The diagrams on the right-hand side present the cross sections along the horizontal dashed-dotted lines in the corresponding pseudocolor plots. The positions of these lines have been chosen at the peak maxima. Figure 6 demonstrates that the scattering intensity is strongly increasing with the initial film thickness δ .

The diagram in Fig. 7(a) presents the scattering intensity profile as a function of the wave number (spectrum at the moment of highest intensity). The intensity maximum is near a wave number of $q_{\text{max}} \approx 0.8 \times 10^6 \text{ m}^{-1}$ in all films, independent of the film thickness. The observation that the spectral shape and the maximum position are not dramatically altered with film thickness may be an indication that multiple scatterings in thick films do not change the characteristics substantially. According to Eq. (5), the maximum corresponds to a spectrum of undulation wavelengths centered on $\lambda \approx 8 \mu\text{m}$. The diagrams also show that the scattering profile shifts to larger wave numbers with time.

Figure 7(b) shows the scattering intensity profile at a later stage, after the rim has passed the laser beam (cross sections along vertical lines in the pseudocolor plots in Fig. 6). It demonstrates an astonishing observation. There is still mea-

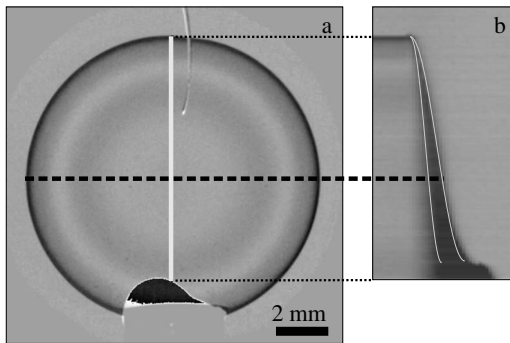


FIG. 8. Estimation of the propagation speed of undulations from the velocity of the dark front. (a) shows the initial image of the nonpunctured bubble (diameter of 1.12 cm and film thickness of $2.38 \mu\text{m}$), background corrected and contrast enhanced. (b) is a space-time plot of vertical cross sections [along the bright vertical line in image (a)] constructed from 42 images. The total time range is 7.0 ms, images were taken with a rate of 6 images/ms. Two bright curves in (b) mark the progression of the rim (right) and of the dark front (left) (see text).

surable scattering, even though the liquid film has gone. We emphasize that this is no camera artifact. In fact, the spectrum of the scattering profile is clearly shifted after the rim passage. This residual scattering might indicate the existence of small liquid droplets generated by fragmentation of the rim during rupture [20].

The space-time plot in Fig. 8(b) has been constructed from an image sequence taken during rupture. It combines the central vertical profiles [cf. white line in Fig. 8(a)] of the individual images. The time axis runs from left to right. The position of the rim is marked by a white curve in image (b). Constant rim velocity has been assumed. Since the rim moves approximately on a spherical surface, the line representing its vertical position vs time appears cosine shaped. The best fit is $v_{\text{rim}}=4.8 \text{ m/s}$. The second white line in (b) marks the approximate position of a dark front, which precedes the rim. This front is not sharp. We have defined it here as the position where the transmitted intensity has dropped to one half of its original value. Again, the cosine shape corresponds to a constant velocity of this front on the spherical surface. The average velocity of this front is 10 m/s, but there is a noticeable darkening already before that (left of the second white line). Due to the experimental uncertainty, this value reflects only a lower limit of the progression speed of peristaltic undulations.

C. Calculation of light transmission through an undulated smectic film

A calculation of the transmission characteristics supports the assumption that traveling waves of the peristaltic type are responsible for the light scattering. The optical transmission of a plane, normally incident wave through a free standing film has been calculated, and the light intensity profile has been determined in the near field. The calculation is performed with finite element method, using the software COMSOL 3.4. This method solves the complete Maxwell

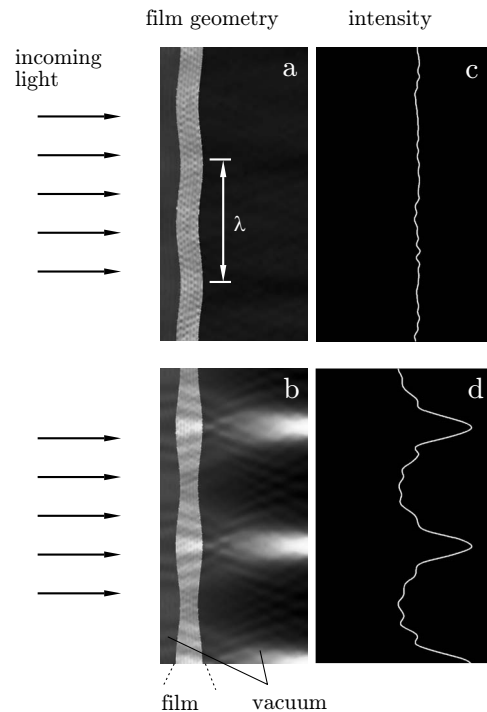


FIG. 9. Calculated transmission of parallel, normally incident light through an undulated film with $\delta=1.5 \mu\text{m}$. The two situations of (a) symmetric and (b) antisymmetric undulations of the surfaces are clearly distinguishable by their optical transmission characteristics. The corresponding transmission profiles are plotted in the two graphs on the right-hand side.

equations numerically on a grid, using a two-dimensionally inhomogeneous and anisotropic optical matrix. The two geometries under consideration can be seen in Figs. 9(a) and 9(b). The planar films modulated with a capillary undulation wave [Fig. 9(a)] and a peristaltic wave [Fig. 9(b)] are indicated in the left-hand side of the figure (the light intensity distribution in the film has been artificially enhanced in the plot for visualization). The period of the modulation in both cases has been assumed to be $\lambda \sim 8 \mu\text{m}$ and ordinary and extraordinary refractive indices are taken as $n_o=1.5$ and $n_e=1.65$, respectively. The films are surrounded by an optical medium with refractive index of 1. The director field is assumed as continuous, the optic axis at the liquid crystal to air interface is perpendicular to the surface. In the calculations, the undulation amplitude was 10%. In practice, it may be only 1% or smaller. The deflection of light will be correspondingly weaker, but qualitatively the same.

A plane wave of wavelength $\lambda_0=670 \text{ nm}$ starts from the left. It is obvious that only the peristaltic wave causes a sufficiently strong deflection of light to be responsible for the opacity of the films during rupture. On the right-hand side of Fig. 9, the respective intensity profiles at the right-hand border of the calculated areas [(a) and (b)] are shown.

The film with constant thickness in (a) does scatter transmitted light. The optical wave remains plane and except for numerical fluctuations the calculation produces plane waves at the opposite film side. Even if such undulation waves would propagate in the bursting films ahead of the rim, they would not be detected optically. In contrast, the peristaltic

undulations in (b) cause a focusing, strongly dependent on the undulation amplitude. The antinodes act lenslike and the whole film behaves like a lattice. The calculations describe only the near field and have no direct quantitative relation to the observed scattering profile. However, it can be concluded from the numerical analysis of light propagation through both types of film profiles that scattering will be observable in the far field as well when peristaltic modulations of the film are present, while the film does not scatter in the case of symmetric surface undulations.

After puncture, we assume that a broad spectrum of waves with different propagation directions is generated in the film. This spectrum manifests itself optically in a strong scattering of the transmitted light, without azimuthal preferences, leading to the extinction of the light in transmission and to a brightening of the film when it is observed under indirect illumination.

IV. ESTIMATION OF THE VELOCITY OF PERISTALTIC MODULATIONS

In order to find an estimate for the velocities of peristaltic waves, we recollect the equations describing the dynamics of a smectic film [16,25]. The continuity equation is

$$\partial_x v_x + \partial_z v_z = 0. \quad (6)$$

From the Navier-Stokes equation, under consideration of only the linear terms, one obtains

$$\rho \partial_t v_x = -\partial_x p + \partial_x \sigma'_{xx} + \partial_z \sigma'_{xz}, \quad (7)$$

$$\rho \partial_t v_z = -\partial_z p + \partial_x \sigma'_{zx} + \partial_z \sigma'_{zz} + B \partial_z^2 u - K \partial_x^4 u \quad (8)$$

with the viscous stress tensor σ'_{ij} and pressure p . For simplicity we have dropped the indices of the splay elastic constant. The time derivative of the layer displacement can be related to the velocity component normal to the film plane and to permeation of the mesogens through the layer borders by

$$\rho \partial_t u = v_z + \lambda_p (B \partial_z^2 u - K \partial_x^4 u), \quad (9)$$

where λ_p is a permeation constant [37]. Several authors [27–31] have calculated dynamic modes on free standing films by solving the dynamic equations with different approaches and different approximations. The first approach, used, e.g., by Chen and Jasnow [29], is a continuum hydrodynamic description of the film dynamics. The internal layer structure is considered by an elastic term that contains the smectic layer compression modulus. The authors describe the dynamics of the surfaces and of the smectic layers in thin freely suspended smectic films under external forcing [29]. Their model shows that the two modes mentioned above, undulation and peristaltic, are essential for the dynamics of the film surfaces. Other modes, influenced by the permeation of molecules, are necessary to fulfill the boundary conditions, but they are not essential for the dynamics of the film surfaces. Two characteristic lengths are defined which determine the limits of applicability of the thin film dynamics. For the peristaltic waves, a graphical solution is given for the wave-vector component normal to the film plane, and a

dispersion relation is derived for waves of both types traveling on the film.

Poniewierski *et al.* [27] introduced a different strategy. They treat the dynamics of the individual film layers as a set of elastically coupled membranes and they solve a differential equation system with a set of equations corresponding to the number of smectic layers. The solution is presented in the form of a discrete set of eigenmodes which are distinguished by the wave-vector component in the direction of the film normal. The discrete model is used also, e.g., by Romanov and Ul'yanov [28,30]. The authors show how the differential equation system can be derived from the continuous hydrodynamic description. Their approach may represent a more realistic picture of the internal microscopic film structure.

The relation between angular frequency ω and in-plane wave vector q of pure undulation waves of the film is given by

$$\omega = \sqrt{\frac{2\gamma}{\rho\delta}} q$$

[cf. Eq. (2), the layer structure is irrelevant] and their damping rate is [30]

$$\frac{1}{\tau} = \frac{\eta_3 q^2}{2\rho}.$$

The peristaltic waves, with nonzero wave-vector component k in the direction of the film normal, have larger frequencies. These depend on k and the ratio $\sqrt{B/\rho}$ which is related to the velocity for “second sound” waves on a smectic-A film [37] (see below).

Being interested in a first approximation of the velocity of mechanical waves on the film, we will perform a simplified calculation. We start with the same differential equations as in [29,30] but we will neglect dissipation and thus set all terms containing viscosities to zero. This is equivalent to the assumption that $\omega\tau \ll 1$. The approximation can be justified by a comparison of $1/\tau$, the velocities of undulation and peristaltic waves, and the wavelengths in the micrometer range and comparable film thicknesses. For the description of dynamic light scattering (e.g., [23]) or x-ray scattering spectra, this approximation is of course unsuitable since the dissipative terms determine the amplitude of thermally excited fluctuations. For our purpose, an experimental justification of this simplification is the fact that the mechanical waves of the second peristaltic type spread over the whole film surface rather uniformly; they are not damped quickly. Otherwise, scattering would be concentrated to the vicinity of the progressing rim.

With the approximations mentioned, the Navier-Stokes equation reduces to

$$\rho \partial_t v_x = -\partial_x p, \quad (10)$$

$$\rho \partial_t v_z = -\partial_z p + B \partial_z^2 u - K \partial_x^4 u. \quad (11)$$

The splay elastic term is dropped in the following because its contribution is negligible in comparison to the layer compressibility term for wavelengths in the micrometer range. We will also neglect permeation of molecules between neighboring layers, $\lambda_p=0$, and Eq. (9) simplifies to

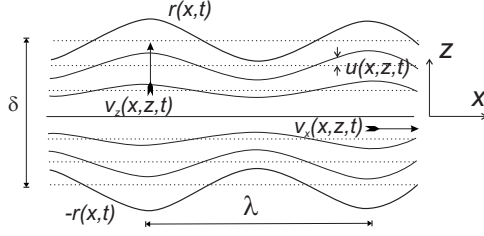


FIG. 10. Schematic presentation of the geometry of a peristaltic wave in a free standing smectic film and sketch of the layer displacement and velocities.

$$\rho \partial_t u = v_z. \quad (12)$$

The equations will be solved with the ansatz

$$v_x = \hat{v}_x \cos kz \exp i(\omega t - qx), \quad (13)$$

$$v_z = i\hat{v}_z \sin kz \exp i(\omega t - qx), \quad (14)$$

$$p = \hat{p} \cos kz \exp i(\omega t - qx) + p_0, \quad (15)$$

$$u = \hat{u} \sin kz \exp i(\omega t - qx). \quad (16)$$

We eliminate the two velocity components with the help of Eqs. (6) and (10)

$$\hat{v}_x = \frac{q}{\omega\rho} \hat{p}, \quad \hat{v}_z = \frac{q}{k} \hat{v}_x = \frac{q^2}{\omega\rho k} \hat{p} \quad (17)$$

and obtain two equations relating pressure and layer displacement:

$$(q^2 + k^2)\hat{p} = Bk^3\hat{u}, \quad (18a)$$

$$\omega\hat{u} = \frac{q^2}{\omega\rho k} \hat{p}. \quad (18b)$$

The boundary conditions for the stress tensor σ_{ij} at the upper and lower film surfaces are

$$\sigma_{xz} = \sigma_{xz}^{\text{ext}} = 0, \quad (19)$$

which is always fulfilled in our model where viscosities have been disregarded, and

$$\sigma_{zz} = \sigma_{zz}^{\text{ext}} \pm \gamma \partial_x^2 \zeta^\pm = -P^\pm + B \partial_z \zeta^\pm, \quad (20)$$

where $\zeta^\pm = u(\pm r)$ and $P^\pm = p(\pm r)$ are layer displacement and pressure, respectively, at the film surfaces (Fig. 10),

$$P^\pm = \hat{p} \cos kr \exp i(\omega t - qx),$$

$$\zeta^\pm = \pm \hat{u} \sin kr \exp i(\omega t - qx),$$

$$\sigma_{zz}^{\text{ext}} = -p_0.$$

The second boundary condition leads to a relation $\hat{p} = (\gamma q^2 \tan kr + Bk)\hat{u}$, and finally, with the help of Eq. (18a), to the transcendental equation

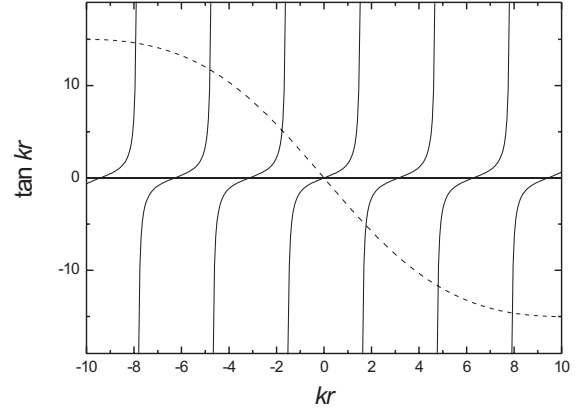


FIG. 11. Graphical solution of Eq. (21). Allowed values for kr are found from the intersections of $\tan kr$ (solid lines) with $Bk/(\gamma(q^2+k^2))$ (dashed line). Typical values for B and γ (see text) have been used for demonstration.

$$-\frac{Bk}{\gamma(q^2+k^2)} = \tan kr, \quad (21)$$

which can be used to establish a relation between the normal and in-plane wave vector components k and q . This equation may be solved graphically, as shown exemplarily in Fig. 11.

Because of the relation $Bk \gg \gamma(q^2+k^2)$, for B on the order of 10^7 Pa, γ on the order of 0.02 N/m, and wave numbers in the range of 10^6 m $^{-1}$, the argument of the tangent is near $\pi/2$ [in general $(n-1/2)\pi$ with n integer]. Thus $k \approx \pi/\delta$ will be only weakly dependent on the in-plane wave vector q . Inserting this result in Eqs. (18a) and (18b), one finds a dispersion relation

$$\omega = \sqrt{\frac{B}{\rho} \frac{kq}{\sqrt{k^2+q^2}}} \approx \sqrt{\frac{B}{\rho} \frac{1}{\sqrt{1+\delta^2 q^2 \pi^{-2}}}} q \quad (22)$$

for the $n=1$ mode.

Figure 12 shows the q dependence of the phase velocity ω/k for $n=1$ and group velocities $d\omega/dk$ for $n=1, 2, 3$ calculated with the model. The maximum velocity of second sound is given by $\frac{1}{2}\sqrt{B/\rho}$ [37]; therefore, a discussion of the result is necessary. In our definition, $v_{\text{ph}} = \omega/q$ describes the

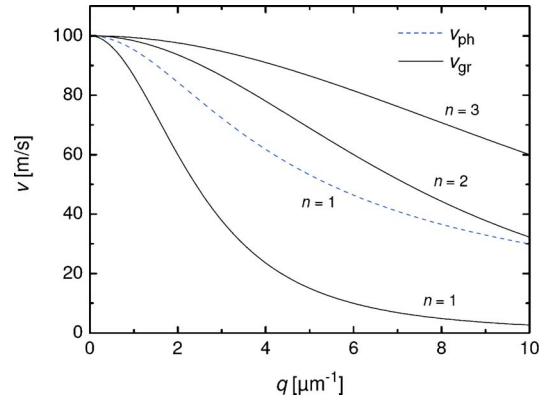


FIG. 12. (Color online) Examples of calculated phase and group velocities of peristaltic waves in dependence on their wave number; n is the mode in z direction. $B=10^7$ Pa and $\gamma=0.03$ N/m have been assumed.

propagation of the phase in the film plane according to Eqs. (13)–(16), which actually results from the superposition of two waves with wave vectors $\vec{q}_{\pm} = (q, \pm k)$ oblique to the film plane. Their phase velocity is lower, $\omega k q / (k^2 + q^2)$, but is not relevant for the propagation of undulations in the film plane.

V. DISCUSSION AND SUMMARY

In this paper, we have analyzed the question why smectic bubbles become opaque during rupture, whereas soap films of comparable thickness remain transparent, even though they burst with comparable velocities. The scattering of smectic bubbles can be explained when one assumes a propagation of second sound waves in the smectic films. Such waves can appear in the films as a consequence of the smectic layer structure and the compression or dilatation elasticity of the layers. We assume that these mechanical waves are continuously initiated by the impact of the moving rim at the film edge on the resting film, even though the detailed mechanism could not be resolved within this study. Culick's [4] and Taylor's [5] considerations showed that the surface energy released from the retracting film edge is not completely converted into kinetic rim energy. Approximately half of the surface energy must be transformed into other energy forms. Most of this excess energy is dissipated, but it is reasonable to assume that some part of this excess is the source for the generation of elastic waves in the remnant film. It is clear that the energy for the formation of peristaltic waves does not reduce the kinetic energy of the rim (which is more or less determined by the assumption of the validity of the momentum balance), so the rim will not be noticeably slower than that of bursting soap films.

The following experimental evidence supports our interpretation: after rupture, thick films, i.e., films with thickness on the order of ≈ 200 smectic layers and above, become opaque. The darkening spreads frontlike along the film, starting from the position of film puncture. When observed under indirect illumination, the films become brighter during rupture. This indicates that light scattering is responsible for the opacity. The observed wave fronts propagate with some finite speed, and they cannot over-run large film thickness steps (steps where the change in film thickness is on the order of the film thickness itself). When films of inhomogeneous thickness burst, the different regions become opaque sequentially. In each uniform region darkening starts with the transgression of the film across the thickness step. The peristaltic waves are either reflected or absorbed at sufficiently large film thickness steps. We assume that they are reflected at the film regions with larger mass per area.

The rupture experiment described here appears to be a convenient method to excite large amplitude undulation waves. From a back of the envelope calculation, we may estimate the undulation amplitudes of the films. The surface energy released at the edge per time and unit length ℓ is given by $w_{\text{surf}} = 2\sigma v_c$. Approximately half of this energy per length is stored in the rim as kinetic energy. The rest, on the order of 0.1 N/s is dissipated and to a small part emitted as peristaltic waves. If we assume an elastic energy per volume of $\langle \frac{1}{2} B u_z^2 \rangle = \frac{1}{8} B (\hat{u} k)^2$ in the peristaltic waves ($\langle \rangle$ means spatial

averaging) and consider that the kinetic-energy density $\frac{1}{8} \rho (\hat{v}_x^2 + \hat{v}_y^2)$ is on the same order of magnitude as the elastic potential energy in the waves, we can estimate their maximum undulation amplitude. The film thickness varies with $\delta + 2\hat{\zeta}(x) \exp i(\omega t - qx)$, where $\hat{\zeta} \ll \delta$. In modes with $kr \approx (2n + 1)\pi/2$ (cf. Fig. 11), the amplitude of the film thickness undulations $2\hat{\zeta}$ is approximately $2\hat{u}$. The peristaltic wave transports an elastic energy of approximately

$$w_{\text{elast}} = \frac{1}{2} B (\hat{\zeta} k)^2 v_{\text{ph}} \delta$$

per unit length ℓ and time in the direction of its propagation, and roughly the same amount of kinetic energy. When these terms are equated to the maximum available power density $w_{\text{surf}}/2 \approx 0.1$ N/s, one can estimate an upper limit of

$$\hat{\zeta} < \sqrt{\frac{\sigma v_c}{B k^2 v_{\text{ph}} \delta}} \approx 10 \text{ nm}$$

for a 1- μm -thick film. This is about 1% of the film thickness and of sufficient magnitude to be responsible for the observed scattering.

The wave velocity, as estimated from typical values for the smectic layer compression modulus B [40] and from the mass density ρ of about 10^3 kg/m³, is much faster than the rupture velocity of the films. We estimate the velocity of the peristaltic waves to be on the order of 10–100 m/s. The largest uncertainty of the estimation is the layer compression modulus of the material. This coefficient can be accessed, e.g., by Rayleigh scattering [41] or from mechanical vibrations of smectic surfaces [42]. Measurements of 8CB homologs have been published, e.g., by Martinoty *et al.* [40,43,44]. The quantity shows a pronounced frequency dependence. It is in the range of 10^6 Pa at low frequencies (subkilohertz), but increases strongly with frequency. In the high-frequency range, for example, values for B in the GHz range determined by Liao *et al.* [45] are about 2 orders of magnitude larger (in the range of 10^9 Pa) than typical low-frequency values. In our experiment, with velocities on the order of 10 m/s and wave numbers of 10^6 m⁻¹, we estimate that the typical frequencies of the wavelengths that contribute to the observed scattering are in the range of a few megahertz.

The fact that in thin films we do not observe pronounced scattering of light during rupture may have two reasons. First, the burst velocity is considerably faster than in thick bubbles, owing to the film thickness in the denominator of the rim velocity. The waves may not move much faster than the rim. Furthermore, the undulation of the surfaces of thin films will be much weaker than in thick films when comparable relative magnitudes of layer compressions are considered. The scattering efficiency is related to the absolute amplitude of the film thickness modulations; thus, the effect will be much weaker. The wavelength peak in the scattering spectrum is slightly shifted with lowering film thickness, but this effect is not dramatic. It is not expected that this shift is the reason for the disappearance of the scattering effect in thin films. Rather, the intensity of scattered light decreases below the detection level.

The observation of some blurred scattering after the rim has passed the laser beam may indicate that some small droplets disintegrate from the rim and form a thin fog. Our observation technique does not allow us to obtain a clear direct evidence of such a fog. At least, its existence might partially explain the slight deviations of measured rim velocities [19] from Culick's prediction. The analysis of the microscopic rim shape and disintegration phenomena of the rim remain unresolved questions of smectic film bursts.

Finally, it is evident that soap bubbles, which behave in several respects quite similar to smectic films, cannot show the observed scattering effect during their bursts. The lack of internal molecular layers prevents the propagation of second sound waves as described in the present model.

Summarizing, the proposed model can explain the experimental observations consistently. The quantitative measure-

ment of material parameters (such as the layer compression modulus) is impossible with this experiment since the wave velocities are difficult to determine quantitatively.

Smectic-A films represent the simplest smectic structures and the description of their dynamics is particularly straightforward. In smectic-C* films (with the commercial mixture Felix 16-100 from Clariant), we observe a qualitatively similar darkening during rupture. However, the situation is much more complex there since the tilt angle may be involved in modulations of the smectic layers.

ACKNOWLEDGMENTS

The authors would like to thank Ulrike Kornek for her collaboration in some of the experiments. We are grateful to Pawel Pieranski for fruitful discussions. We acknowledge financial support by the DFG under Grant No. STA 452/20.

-
- [1] A. Dupré, *Théorie Mécanique de la Chaleur* (Gauthiers-Villars, Paris, 1869).
- [2] A. Dupré, *Ann. Chim. Phys.* **11**, 194 (1867).
- [3] Lord Rayleigh (W. Strutt), *Scientific Papers* (Cambridge, UK, 1902), Vol. 3, 441.
- [4] F. E. Culick, *J. Appl. Phys.* **31**, 1128 (1960).
- [5] G. Taylor, *Proc. R. Soc. London, Ser. A* **253**, 313 (1959).
- [6] W. E. Ranz, *J. Appl. Phys.* **30**, 1950 (1959).
- [7] W. R. McEntee and K. J. Mysels, *J. Phys. Chem.* **73**, 3018 (1969).
- [8] S. Frankel and K. J. Mysels, *J. Phys. Chem.* **73**, 3028 (1969).
- [9] L. J. Evers, S. Y. Shulepov, and G. Frens, *Phys. Rev. Lett.* **79**, 4850 (1997).
- [10] J. Evers, E. J. Nijman, and G. Frens, *Colloids Surf., A* **149**, 521 (1999).
- [11] A. B. Pandit and J. F. Davidson, *J. Fluid Mech.* **212**, 11 (1990).
- [12] P. Pieranski *et al.*, *Physica A* **194**, 364 (1993).
- [13] J. C. Geminard, R. Hołyst, and P. Oswald, *Phys. Rev. Lett.* **78**, 1924 (1997).
- [14] P. Oswald, P. Pieranski, F. Picano, and R. Hołyst, *Phys. Rev. Lett.* **88**, 015503 (2001).
- [15] F. Picano, P. Oswald, and E. Kats, *Phys. Rev. E* **63**, 021705 (2001).
- [16] F. Picano, R. Hołyst, and P. Oswald, *Phys. Rev. E* **62**, 3747 (2000).
- [17] F. Caillier and P. Oswald, *Eur. Phys. J. E* **20**, 159 (2006).
- [18] P. Oswald and P. Pieranski, *Smectic and Columnar Liquid Crystals* (Taylor & Francis, Boca Raton, FL, 2006).
- [19] F. Müller, U. Kornek, and R. Stannarius, *Phys. Rev. E* **75**, 065302(R) (2007).
- [20] F. Müller and R. Stannarius, *Liq. Cryst.* **36**, 133 (2009).
- [21] J. Lucassen, M. Van den Tempel, A. Vrij, and F. Th. Hesselink, *Proc. K. Ned. Akad. Wet., Ser. B: Phys. Sci.* **73**, 109 (1970).
- [22] Y. Couder, J. M. Chomaz, and M. Rabaud, *Physica D* **37**, 384 (1989).
- [23] A. Böttger and J. G. H. Joosten, *Europhys. Lett.* **4**, 1297 (1987).
- [24] W. H. de Jeu, B. I. Ostrovskii, and A. N. Shalaginov, *Rev. Mod. Phys.* **75**, 181 (2003).
- [25] P. C. Martin, O. Parodi, and P. S. Pershan, *Phys. Rev. A* **6**, 2401 (1972).
- [26] R. Hołyst, D. J. Tweet, and L. B. Sorensen, *Phys. Rev. Lett.* **65**, 2153 (1990).
- [27] A. Poniewierski, R. Hołyst, A. C. Price, L. B. Sorensen, S. D. Kevan, and J. Toner, *Phys. Rev. E* **58**, 2027 (1998).
- [28] V. P. Romanov and A. N. Shalaginov, *Sov. Phys. JETP* **75**, 483 (1992).
- [29] H. Y. Chen and D. Jasnow, *Phys. Rev. E* **57**, 5639 (1998); **61**, 493 (2000).
- [30] V. P. Romanov and S. V. Ulyanov, *Phys. Rev. E* **63**, 031706 (2001); **65**, 021706 (2002).
- [31] V. P. Romanov and S. V. Ulyanov, *Phys. Usp.* **46**, 915 (2003).
- [32] R. Hołyst, *Phys. Rev. A* **44**, 3692 (1991).
- [33] R. Hołyst, *Phys. Rev. A* **46**, 6748 (1992).
- [34] J. D. Shindler, E. A. L. Mol, A. Shalaginov, and W. H. de Jeu, *Phys. Rev. Lett.* **74**, 722 (1995).
- [35] E. A. L. Mol, J. D. Shindler, A. N. Shalaginov, and W. H. de Jeu, *Phys. Rev. E* **54**, 536 (1996).
- [36] A. Madsen, J. Als-Nielsen, and G. Grubel, *Phys. Rev. Lett.* **90**, 085701 (2003).
- [37] P. G. deGennes and J. Prost, *The Physics of Liquid Crystals* (Clarendon, Oxford, 1993).
- [38] K. Miyano and J. B. Ketterson, *Phys. Rev. Lett.* **31**, 1047 (1973).
- [39] R. Stannarius, C. Cramer, and H. Schüring, *Mol. Cryst. Liq. Cryst. Sci. Technol., Sect. A* **350**, 297 (2000).
- [40] P. Martinoty, J. L. Gallani, and D. Collin, *Phys. Rev. Lett.* **81**, 144 (1998).
- [41] J. D. Litster, J. Als-Nielsen, R. J. Birgeneau, S. S. Dana, D. Davidov, F. Garcia-Golding, M. Kaplan, C. R. Safinya, and R. Schaezting, *J. Phys. (Paris), Colloq.* **40**, C3-339 (1979).
- [42] M. R. Fisch, L. B. Sorensen, and P. S. Pershan, *Phys. Rev. Lett.* **47**, 43 (1981).
- [43] D. Rogez, D. Collin, and P. Martinoty, *Eur. Phys. J. E* **14**, 43 (2004).
- [44] D. Rogez, L. G. Benguigui, and P. Martinoty, *Eur. Phys. J. E* **16**, 193 (2005).
- [45] Y. Liao, N. A. Clark, and P. S. Pershan, *Phys. Rev. Lett.* **30**, 639 (1973).